August 2003

THE SPECTRA OF TYPE II CEPHEIDS. I. THE Hα LINE IN SHORT-PERIOD STARS

Edward G. Schmidt
University of Nebraska-Lincoln, eschmidt1@unl.edu

Kevin M. Lee
University of Nebraska-Lincoln, klee6@unl.edu

Dale Johnston
University of Nebraska-Lincoln, dalej96@bigred.unl.edu

Peter R. Newman
New Mexico State University, prn@apo.nmsu.edu

Stephanie A. Snedden
New Mexico State University, snedden@apo.nmsu.edu

The Astronomical Journal, 126:906–917, 2003 August

THE SPECTRA OF TYPE II CEPHEIDS. I. THE Hα LINE IN SHORT-PERIOD STARS[1]

Edward G. Schmidt,[2] Kevin M. Lee,[2] and Dale Johnston[2]
Department of Physics and Astronomy, University of Nebraska–Lincoln, Lincoln, NE 68588-0111;
eschmidt1@unl.edu, klee6@unl.edu, dalej96@bigred.unl.edu

and

Peter R. Newman and Stephanie A. Snedden
Apache Point Observatory, P.O. Box 59, Sunspot, NM 88349-0059;
and Department of Astronomy, New Mexico State University, P.O. Box 30001, Las Cruces, NM 88003-8001;
prn@apo.nmsu.edu, snedden@apo.nmsu.edu
Received 2003 April 28; accepted 2003 May 12

ABSTRACT

We present 88 Hα profiles for 24 pulsating variable stars with periods between 1 and 3 days in order to explore the behavior of this line in type II as compared with classical Cepheids. Surprisingly, large velocity differences were found between Hα and the metal lines in some type II Cepheids. Strong emission was observed in three stars, VZ Aql, NW Lyr, and V439 Oph, while line filling by incipient emission is present in seven others. All of the stars with emission and most with incipient emission belong to Diethelm's AHB2 class, and the emission is associated with the secondary bump on the rising branch of the light curve. Two stars, BF Ser and MQ Aql, show doubling of the core near maximum light, and asymmetry of the line is noted in some spectra.

Key words: Cepheids — stars: Population II

1. INTRODUCTION

Since the pioneering studies of Joy (1949), it has been known that the spectra of long-period type II Cepheids (also referred to as W Virginis stars and classed as CWA in the General Catalogue of Variable Stars [GCVS; Kholopov 1985, 1987]) and RV Tauri stars often exhibit strong emission lines of hydrogen, particularly Hα (see, e.g., Kraft, Camp, & Hughes 1959; Lèbre & Gillet 1992; Pollard et al 1997). In the case of the short-period type II Cepheids (also known as BL Herculis stars and classed as CWB in the GCVS), relatively weak hydrogen line emission has been reported (Abt & Hardie 1960; Preston & Kilston 1967; Gillet et al. 1994; Vinko et al. 1998) but appears to be rather uncommon (see, e.g., Harris & Wallerstein 1984). Although Loomis & Schmidt (1989) reported strong Hα emission in the spectrum of HR Aur ($P = 1.63$ days), they concluded that the GCVS classification of CWB was in error; it is probably an interacting binary. The behavior of type II Cepheids is in contrast to that of the classical Cepheids, where hydrogen emission seldom occurs and is very weak when it does (Schmidt 1970).

Other indications of the different behavior of the atmospheres of type II as compared with type I Cepheids are found in the velocity differentials between Hα and the photospheric metal lines and by doubling of the core of Hα. Vinko et al. (1998) have summarized these phenomena for stars with periods less than 10 days.

While these previous studies have provided a broad outline of the behavior of Hα in type II Cepheids, the number of stars included has been too limited to provide a detailed picture. In addition, some of the earlier studies employed photographic spectra, which suffer from poor signal-to-noise ratios and nonlinearity. To address these shortcomings, we undertook a spectral survey using modern detectors. Most of the approximately 85 stars in the survey were drawn from the CWA and CWB stars in the GCVS, but we also included some classed as CEP (Cepheids of uncertain type) to expand the sample and some classed as DCEP (classical Cepheids) to provide comparisons. In this paper, we present and discuss 88 spectra of the 24 shortest period stars in the sample ($P < 3$ days). These stars include about 70% of the CWB stars in the GCVS with periods less than 3 days accessible from Behlen Observatory, where the photometry for this program is being conducted.

2. OBSERVATIONS

The stars discussed here are listed in Table 1, where column (1) gives the names of the stars, and column (2) their classification from the GCVS. Column (3) lists the metallicity from Harris (1981a, 1981b), Harris & Wallerstein (1984), or Diethelm (1990). There are only a half-dozen stars in common between the first three sources and the fourth. Excluding one outlier, the abundance scales agree closely, with a scatter of less than 0.5 dex. Columns (4) and (5) list the periods and epochs used to calculate phases for the spectra. These were determined from the photometry referenced in the last column. For most of the stars, we have recent photometry, which will be published at a later time. We are confident of the phasing of the spectra of these stars, while the phases for the others should be treated with caution. In column (6), the phase of minimum light relative to these ephemerides is listed. For relatively flat-bottomed light curves, the minimum is difficult to locate with certainty in the presence of scatter. In those cases, the point at which the rise toward maximum appeared to begin was selected. In

[1] Based in part on observations obtained with the Apache Point Observatory 3.5 m telescope, which is owned and operated by the Astrophysical Research Consortium.

[2] Visiting Astronomer, Kitt Peak National Observatory, National Optical Astronomy Observatory, which is operated by the Association of Universities for Research in Astronomy, Inc., under cooperative agreement with the National Science Foundation.

TABLE 1
PROGRAM STARS

Star (1)	GCVS Class (2)	[Fe/H] (3)	Period (4)	Epoch of Maximum[a] (5)	Phase of Minimum (6)	ΔV (7)	L. C. Type (8)	Source of Photometry (9)
BF Ser	CWB	−2.5	1.165439	51,241.71	0.90	1.40	AHB1	1, 2, 3
CE Her	CWB	−1.8	1.2094357	46,583.78	0.91	1.36	AHB1	1, 4
BL Her	CWB	0.0	1.3074502	52,536.21	0.78	0.88	(AHB3)	1, 3, 5, 6
VX Cap	CWB	−1.0	1.3275583	41,898.85	0.89	1.30	AHB1	7
MQ Aql	CWB	...	1.48078	52,534.72	0.85	1.18	(AHB1)	2, 3
SW Tau	CWB	0.3	1.58356	51,914.42[b]	0.60[b]	0.82	AHB3	3, 5, 6, 8, 9
V745 Oph	CWB	−0.7	1.59558	52,038.69	0.69	0.92	AHB2	3, 7
NW Lyr	CWB	−0.1	1.601179	52,089.87	0.69	1.13	(AHB2)	3, 10
V971 Aql	CWB	−0.3	1.62453	52,500.45[c]	0.69	0.89	AHB2	3, 7
VZ Aql	CWB	0.3	1.66828	52,488.70	0.65	0.92	AHB2	3, 7
V714 Cyg	CWB	...	1.88744	52,425.73	0.70	1.27	(AHB2:)	2, 3
V439 Oph	CWB	−0.3	1.89301	52,447.63	0.70	0.83	AHB2	3, 8, 11, 12, 13
V477 Oph	CWB	−0.5	2.01567	51,829.56	0.74	0.88	AHB2	3, 7, 14, 15
EK Del	CEP	−1.1	2.04686	52,164.36	0.79	0.93	AHB1	3, 7
FF Aur	DCEP	−0.3	2.12056	48,574.75	0.85	1.13	(AHB1)	5, 6, 8, 14, 16, 17, 18
UY Eri	CWB	−1.4	2.21331	52,522.42	0.78	0.71	AHB1	1, 3
BB Gem	DCEP	...	2.308207	52,639.78	0.81	1.08	Cδ	3, 4, 5, 8
AU Peg	CEP	1.5	2.4051	44,490.84	0.69	0.35	(SA)	1, 5, 6, 8
CN CMa[d]	CWB:	0.0	2.54612	52,615.9:	0.6:	0.8:	Cδ	3
EW Aur	DCEP	−0.6	2.65950	52,309.33	0.84	0.90	(AHB1)	1, 14, 19
V351 Cep	CWB	...	2.80652	52,580.61	0.55	0.32	SA	3, 5, 8
V465 Oph	CWB	0.0	2.82194	52,456.88	0.77	1.07	AHB3 or Cδ[e]	3, 7
NY Cas	DCEPS	...	2.82313	52,657.44	0.56	0.48	(SA)	2, 3, 10, 14
BC Aql	CEP	0.1	2.90513	52,485.78	0.81	0.96	Cδ	1, 3

[a] Epochs are listed as Heliocentric Julian Date −2,400,000.

[b] This star has a double hump that makes the identification of the phase of maximum somewhat arbitrary (see Diethelm 1983 for a plot of the light curve). We have taken the second hump that is slightly brighter as the maximum. The first hump, regarded by Diethelm as the maximum, occurs at phase 0.83 with our ephemeris. There is a gradual rise from minimum for about a tenth of a cycle followed by a steep rise to the first hump. We have adopted the beginning of the gradual rise as minimum. The beginning of the rapid rise occurs at phase 0.72.

[c] Based on only two recent photometric measurements.

[d] The period of CN CMa is from Diethelm (1986) based on photographic photometry by Deurinck (1948). The only modern photometry available is a set of seven points from Behlen Observatory. Hence, the epoch, amplitude, and phase of minimum are only approximate.

[e] The type of the light curve is uncertain. This star is included with the AHB3 stars in the discussion.

REFERENCES.—(1) Harris 1980; (2) Henden 1996; (3) unpublished Behlen Observatory photometry; (4) Loomis, Schmidt, & Simon 1988; (5) Szabados 1977; (6) Moffett & Barnes 1984; (7) Kwee & Diethelm 1984; (8) Henden 1980; (9) Barnes et al. 1997; (10) Schmidt & Reiswig 1993; (11) Diethelm & Tammann 1982; (12) Sturch 1966; (13) Harris & Wallerstein 1984; (14) Berdnikov 1987, 1992a, 1992b, 1992c, 1992d, 1992e, 1993; (15) Schmidt & Seth 1996; (16) Berdnikov & Turner 1995; (17) Berdnikov & Voziakova 1995; (18) Kiss 1998; (19) Schmidt, Chab, & Reiswig 1995.

column (7), we give the amplitudes of the V magnitude derived from the same photometry.

Diethelm (1983) identified several types of light curves among short-period Cepheids. He designated stars with smooth light curves and a rapid rise to maximum, reminiscent of the type *ab* RR Lyrae stars, RR*d*. Some stars exhibit a strong hump during rising light and consequently a longer rise time. Diethelm called this group CW. Stars with a hump on the descending branch of the light curve were classed as BL. Finally, stars with a relatively gradual rise to maximum and low galactic latitudes were considered classical Cepheids (Cδ). In a later paper (Diethelm 1990), he renamed the first three groups to avoid confusion with other usages of the same terminology. Assuming all of these stars have evolved off of the horizontal branch, he adopted the notation AHB (above horizontal branch) so RR*d* became AHB1, CW became AHB2, and BL became AHB3. He also added the designation SA for classical Cepheids with nearly sinusoidal light curves. In the latter paper, he also showed that this morphological classification is astrophysically meaningful in that the classes have distinct metallicities that average [Fe/H] $= -1.2 \pm 0.3$ for the AHB1 stars, [Fe/H] $= -0.4 \pm 0.2$ for the AHB2 stars, [Fe/H] $= +0.2 \pm 0.2$ for the AHB3 stars, and -0.1 ± 0.3 for the Cδ stars. This classification will provide a useful structure for our discussion, and we have listed the types in column (8) of Table 1. For those stars not listed by Diethelm (1983, 1990), types were assigned by examination of the light curves and are listed in parentheses.

The spectra were obtained at Kitt Peak National Observatory during 2001 July and 2002 September/October and at Apache Point Observatory during 2002 June. At Kitt Peak, we used the GoldCam Spectrograph on the 2.1 m telescope (Massey et al. 2000).[3] The detector was a Ford 3K × 1K CCD trimmed to 2000 pixels in the direction of dispersion. The spectrograph was configured to produce a dispersion of 0.62 Å pixel^{-1}. The resulting resolution was 2.0 Å, as inferred from the comparison lines near Hα. The useful spectral coverage extended from approximately 5800 to 7070 Å. At Apache Point Observatory, we used the Astrophysical Research Consortium 3.5 m telescope with

[3] Available at http://www.noao.edu/kpno/manuals/l2mspect/spectroscopy.html.

[4] Available at http://www.apo.nmsu.edu/Instruments/DIS/.

the DIS II instrument in spectrographic mode (McMillan, Hastings, & Holtzman 2002).[4] The red channel of this instrument was configured to provide a dispersion of 1.13 Å pixel^{-1} on the Marconi 2048 × 1024 CCD. The resolution was 2.6 Å, and the spectral coverage was from about 5550 to 7480 Å. All the spectra were reduced following standard procedures with the IRAF package.[5]

A log of the spectroscopic observations is given in Table 2, where the stars are identified in column (1), and the Heliocentric Julian Date of mid exposure is given in column (2). The phases relative to maximum light of the observations from the ephemerides of Table 1 are listed in column (3). Column (4) of the table indicates the instrument used to obtain the spectra.

Emission, core doubling, and velocity differentials in Hα are known to be associated with phases of outward acceleration of the atmosphere. This roughly coincides with the interval of rising light, so our observations were preferentially made between minimum light and 0.05 cycles after maximum light. Other phases were opportunistically observed as a second priority. As a result, just over 60% of our spectra were obtained during rising light.

The choice of exposure times was a compromise between the need for a good signal-to-noise ratio (S/N) and the requirement for a relatively large number of spectra to survey our sample. A S/N greater than 50 per resolution element was deemed adequate to measure the important features of the Hα profiles, but we generally tried to achieve a value above 75. We estimated the S/N of our extracted spectra by calculating the rms scatter about a linear fit to the continuum in the band from 6720 to 6820 Å. This assumes that line absorption is negligible in that region compared with the random noise. Since there are always some weak lines, this estimate should be regarded as a lower limit.

Due to the lack of up-to-date ephemerides for some stars, the phases were uncertain, and consequently the magnitudes were uncertain. This, along with variations in the observing conditions, resulted in a range of S/N. For about 90% of our spectra, the estimated S/N exceeds 50, and for about three-fourths of them it exceeds 75. We have included the spectra with an estimated S/N of less than 50 in our analysis, but they are flagged with a footnote in Table 2.

The velocity of the core of Hα relative to the metal lines provides a useful measure of differential velocities in the atmospheres of pulsating stars. The wavelength of Hα was determined by fitting a parabola to several points near the minimum flux of the line or in a few cases the maximum of an emission feature. To determine the wavelength shift of the metal lines, we identified lines in the range from 6100 to 6615 Å that persist at the low metallicities of some of our stars but that remain relatively unblended at solar metallicities. The Na D lines were also used for a few stars where the stellar velocity was sufficiently high to separate the stellar

[5] IRAF is distributed by the National Optical Astronomy Observatory, which is operated by the Association of Universities for Research in Astronomy, Inc., under cooperative agreement with the National Science Foundation.

TABLE 2
Journal of Observations

Star (1)	Mid Exposure HJD −2,452,000 (2)	ϕ (3)	Instrument[a] (4)	ΔVel (5)	Standard Error (6)	Depth of Hα (7)	W_λ (Hα) (8)
BF Ser.....	101.83	0.02	1	−60, 28	22	0.56	7.2
CE Her.....	548.63[b]	0.93	1	9	13	0.44	2.1
	554.66[b]	0.91	1	10	20	0.49	2.3
BL Her.....	101.90	0.82	1	18	5	0.37	2.2
	104.67	0.94	1	17	6	0.61	6.5
	105.76	0.77	1	−13	7	0.56	3.9
VX Cap.....	553.75	0.94	1	−37	20	0.60	6.8
MQ Aql	106.71	0.95	1	−19, 82	9	0.56	6.7
SW Tau.....	546.99	0.46	1	−5	2	0.60	4.5
	551.87	0.54	1	−10	3	0.56	4.2
	551.89	0.56	1	−7	3	0.56	4.1
	551.94	0.59	1	−7	5	0.56	3.9
	551.98	0.62	1	−3	4	0.58	4.4
	553.84	0.78	1	7	3	0.65	6.5
	556.00	0.15	1	−10	3	0.60	5.3
V745 Oph.....	101.88	0.60	1	−45	6	0.50	3.2
	105.68	0.99	1	14	8	0.53	4.8
	106.73	0.64	1	−21	4	0.47	3.2
	443.68	0.82	2	11	8	0.36	3.1
	550.64	0.86	1	−5	5	0.40	2.9
	550.66	0.87	1	1	4	0.38	2.9
	550.68[b]	0.88	1	26	14	0.41	3.7
NW Lyr	105.77	0.93	1	21	4	0.63	4.7
	547.61	0.88	1	32	4	0.53	3.4
	550.71	0.81	1	52 (−50)[c]	6	0.30	2.3
	554.76	0.34	1	−21	3	0.59	3.9
V971 Aql.....	106.77	0.67	1	−24	3	0.43	3.0
	548.61	0.64	1	−16	6	0.46	2.9
	553.60	0.72	1	9	3	0.32	2.2

TABLE 2—*Continued*

Star (1)	Mid Exposure HJD −2,452,000 (2)	ϕ (3)	Instrument[a] (4)	ΔVel (5)	Standard Error (6)	Depth of Hα (7)	W_λ (Hα) (8)
VZ Aql.....	105.88	0.53	1	−35	2	0.49	3.0
	546.68	0.76	1	37 (−61)[c]	5	0.22	1.3
	548.62	0.92	1	25	4	0.61	5.5
	551.62	0.71	1	2	5	0.29	2.1
	553.63	0.92	1	35	4	0.61	5.4
V714 Cyg	104.85	0.99	1	1	8	0.61	6.2
	551.73	0.76	1	−1	4	0.46	3.1
	553.70	0.80	1	34	4	0.47	3.2
	553.79	0.85	1	17	7	0.53	3.4
V439 Oph.....	102.75	0.81	1	(−57)[c]	8	−0.18	0.8
	104.68	0.84	1	63 (−56)[c]	7	−0.10	1.3
	105.68	0.36	1	−11	6	0.48	3.0
	105.86	0.46	1	−36	6	0.48	2.9
	106.65	0.88	1	38	9	0.28	2.2
	106.84	0.97	1	23	6	0.50	4.0
	443.69	0.92	2	39	5	0.40	3.0
V477 Oph.....	101.89	0.11	1	39	17	0.50	4.3
	105.70	0.00	1	68	9	0.37	3.6
	548.65	0.75	1	−7	4	0.57	3.8
	550.67[b]	0.75	1	−62	13	0.42	2.2
	554.68	0.74	1	−40	7	0.40	2.4
EK Del.....	105.90	0.44	1	−23	11	0.47	3.1
	546.75	0.82	1	−14	6	0.54	2.9
	548.80	0.82	1	−25	10	0.55	3.4
FF Aur.....	550.97	0.08	1	−27	7	0.61	5.2
	553.96	0.49	1	2	5	0.55	3.0
UY Eri	546.98	0.10	1	−43	10	0.52	4.2
	548.82	0.93	1	23	10	0.56	4.2
	550.80	0.82	1	4	13	0.47	2.5
	553.86	0.21	1	−37	8	0.50	3.2
	555.86	0.11	1	−22	10	0.50	4.1
BB Gem	546.99	0.80	1	−3	7	0.58	3.4
	551.89	0.92	1	−11	5	0.62	4.3
	553.89	0.79	1	−2	5	0.56	3.3
AU Peg	106.84	0.60	1	−30	4	0.43	2.6
CN CMa.....	556.01	0.48	1	4	3	0.56	2.8
EW Aur	548.86	0.06	1	−25	5	0.60	5.3
	550.86	0.82	1	6	5	0.60	3.0
	551.84	0.18	1	−24	3	0.57	3.9
	553.82	0.93	1	13	3	0.59	3.1
	555.85	0.69	1	2	4	0.59	2.7
V351 Cep	103.81[b]	0.11	1	−32	6	0.58	4.4
	104.99	0.53	1	−3	4	0.54	3.8
	105.73	0.79	1	−1	3	0.56	4.4
	546.76	0.94	1	−14	3	0.60	4.5
	548.78[b]	0.66	1	−10	6	0.53	3.9
	551.76	0.72	1	−6	5	0.57	3.8
	554.71	0.77	1	−5	4	0.60	4.3
V465 Oph.....	547.62	0.16	1	54	4	0.58	4.9
	550.61	0.21	1	67	5	0.59	5.5
NY Cas.....	105.81	0.60	1	−5	8	0.52	3.7
	105.98[b]	0.66	1	−19	6	0.47	3.1
	106.82	0.96	1	−9	3	0.55	4.7
	546.80	0.81	1	−4	5	0.58	4.2
	551.83	0.59	1	0	3	0.54	4.0
	554.81	0.65	1	−9	4	0.54	3.7
	555.96	0.06	1	−18	4	0.59	4.5
BC Aql.....	104.87	0.88	1	14	6	0.36	2.7
	549.61[b]	0.97	1	9	11	0.57	4.6

[a] The instrument used for the observations is either (1) the Gold Spectrograph on the 2.1 m telescope at Kitt Peak National Observatory or (2) DIS II on the 3.5 m Apache Point Telescope.

[b] The lower limit to the S/N less than 50.

[c] Velocities in parentheses refer to an emission peak.

from the interstellar components. For each line in a given spectrum, the central wavelength was determined by fitting a parabola to the core. For the various spectra there were between two and 10 lines that were usable. The internal errors ranged from 7 to 50 km s^{-1} for a single line (with nearly all less than 20 km s^{-1}) resulting in a standard error of the mean for a single spectrum ranging from a few kilometers per second to about 20 km s^{-1}. As would be expected, larger errors are associated with the more metal-deficient stars where fewer lines could be measured and the weak lines produce greater uncertainties.

In column (5) of Table 2, we list the velocity differences between Hα and the metal lines. The standard error in the following column is that calculated for the metal lines, since it dominates over uncertainties in measuring the core of Hα. In a couple of cases, two values are listed reflecting the fact that the core is split. When there is an emission peak within the profile, its velocity is listed in parentheses.

Finally, in column (7) of Table 2, we list the depth of Hα in units of the continuum flux, while in column (8) we list the equivalent width of Hα. The equivalent width was calculated by integrating the area of the line from the central

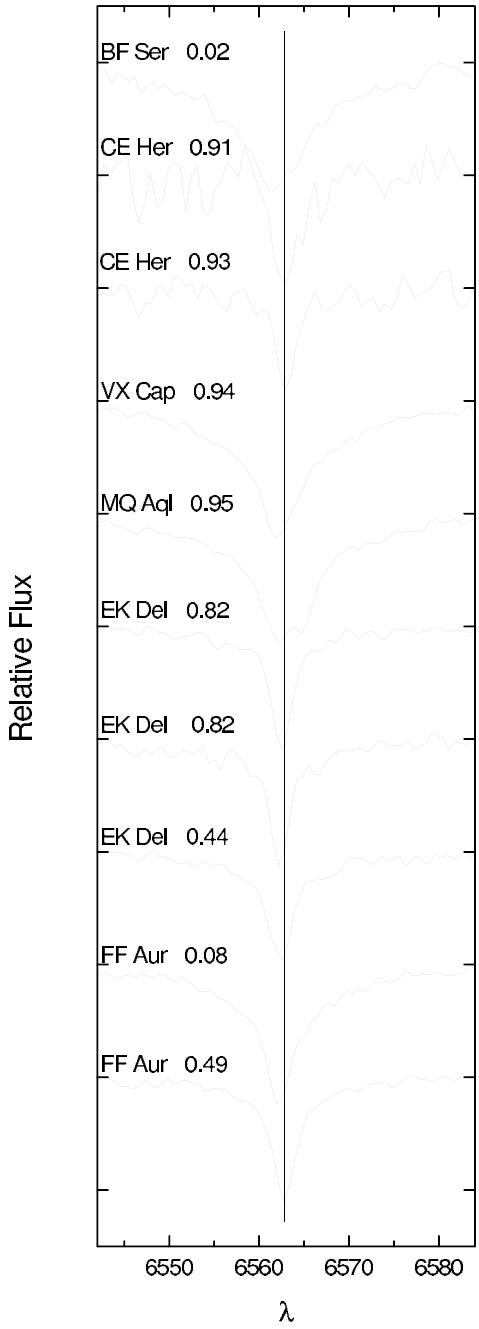

FIG. 1*a*

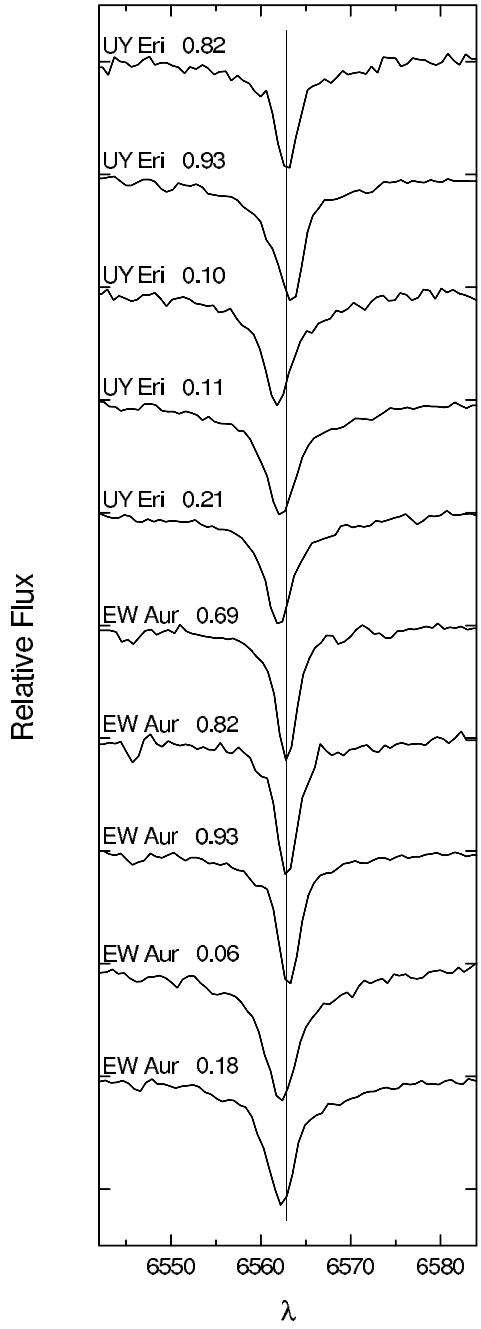

FIG. 1*b*

FIG. 1.—Portion of the spectra near Hα for stars of class AHB1. Each plot is normalized to a continuum level of one and is offset vertically from its neighbors for visibility. The tick marks on the vertical axis are separated by 0.5. Each spectrum is identified by the name of the star and the phase after maximum light. The vertical line indicates the rest wavelength of Hα, and each spectrum has been shifted to the rest frame of the stellar atmosphere as defined by metal lines. Multiple observations of a given star are arranged in order of phase from 0.5 through maximum to 0.5.

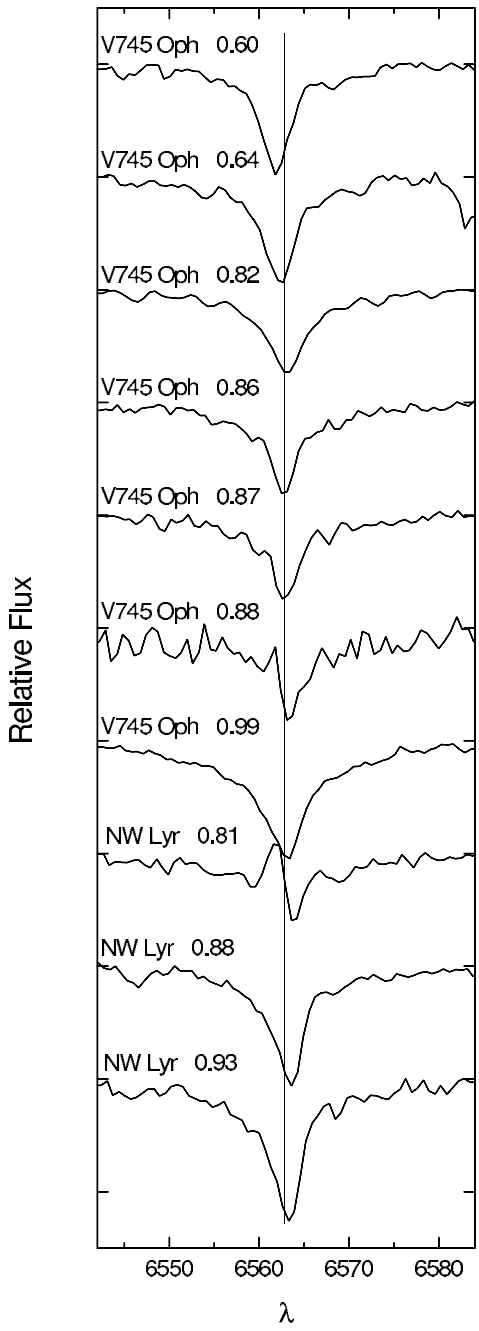

FIG. 2*a*

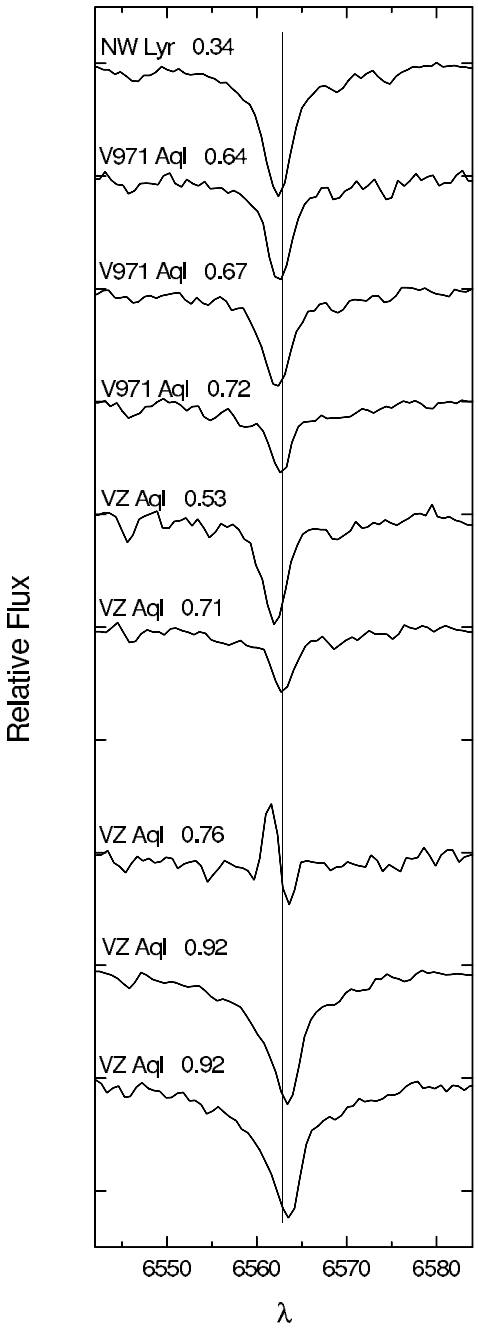

FIG. 2*b*

FIG. 2.—Spectra of the stars of class AHB2. The plot has the same format as Fig. 1.

wavelength outward in steps of 1 Å. When the increase in equivalent width from one step to the next was less than 5%, the integration was stopped. An examination of the spectra indicates that this is a reasonable compromise between incomplete inclusion of the wings of Hα and inclusion of extraneous absorption from other lines. Although the equivalent width is not used in the discussion below, it is included for future reference.

The region of the spectra around Hα is plotted in Figures 1–4. The stars have been grouped according to the Diethelm light-curve types. Each plot is normalized to a continuum level of 1.0 and is offset from its neighbors for visibility. Each spectrum is labeled with name of the star and the phase from maximum light (col. [3] of Table 2). The spectra of multiple observations of individual stars are ordered by phase beginning at 0.5 to facilitate tracing changes before and through maximum. The Hα profiles are plotted in the rest frame of the stellar atmosphere as measured from the metal lines, and the vertical line indicates the rest wavelength of Hα. The differential velocities listed in Table 2 are noticeable in the plots as displacements from the vertical line.

3. DISCUSSION

3.1. *Differential Velocities*

Differential velocities of Hα relative to the metal lines have been reported previously in both type I and type II

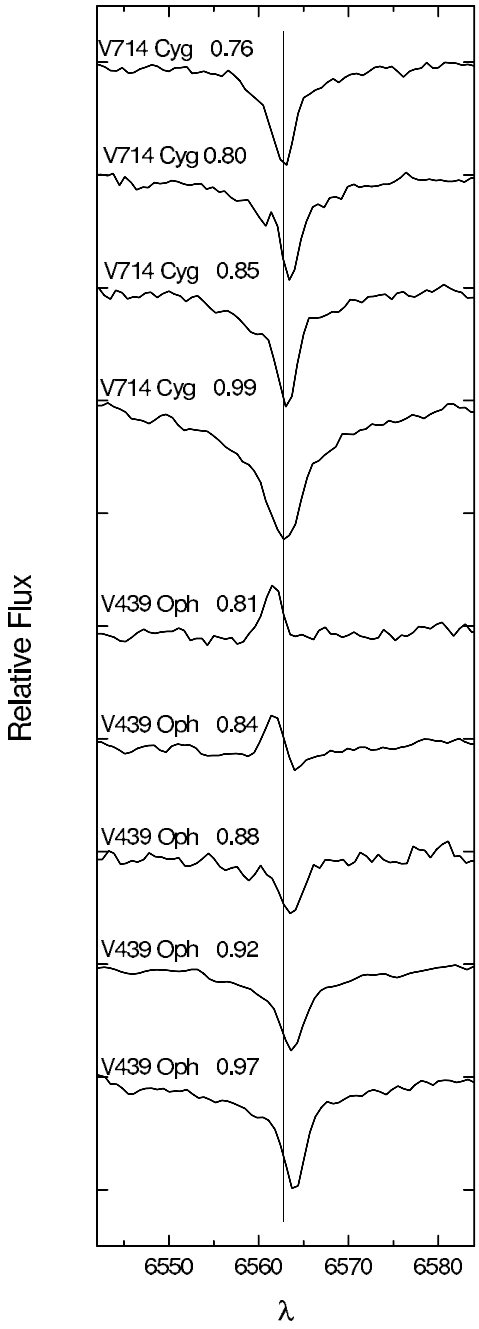

FIG. 2*c*

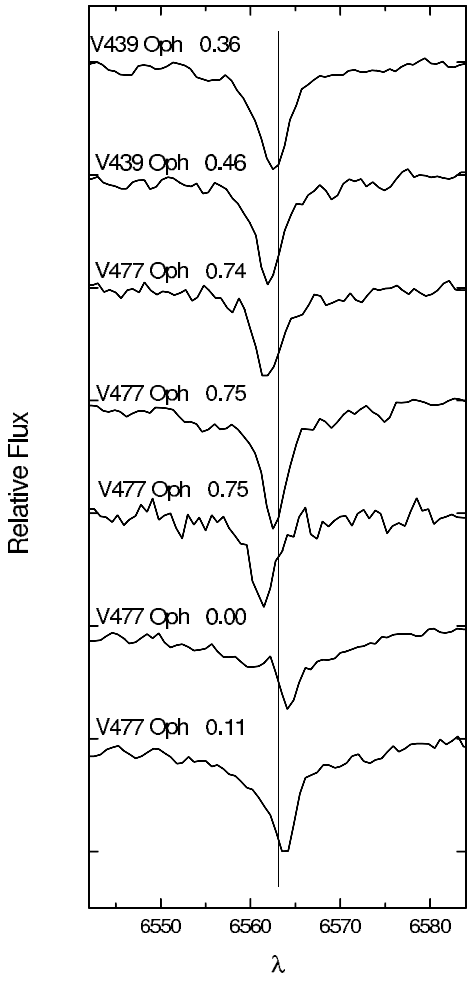

FIG. 2*d*

Cepheids. Vinko et al. (1998) have summarized the behavior of the maximum of the differential velocity over the pulsational cycle, ΔVel_{max}. They showed that it ranges up to 70 km s^{-1} for the stars in their sample and increases with period. However, they included a value of ΔVel_{max} for only one short-period type II Cepheid, BL Her. It had a surprisingly large differential velocity for its period. Note that we have measured the differential velocities for BL Her at three phases and obtained much smaller values. An inspection of Figure 6 of Vinko et al. (1998) shows that the large velocity difference occurred on a single spectrum. Thus, we could have easily missed that phase, although our spectrum at phase 0.94 (see Fig. 3) shows broadening, which may be a precursor to the core doubling that is evident in Vinko et al.'s spectrum just after maximum light.

Since the velocity field in the atmosphere of a pulsating star is generated by the acceleration experienced by the atmosphere, larger values of ΔVel_{max} should be encountered in stars with larger velocity amplitudes. Vinko et al. (1998) explored this by plotting their velocity differentials against the amplitudes in both velocity and magnitude. There is a reasonable correlation of differential velocity with amplitude, and BL Her agrees with the trend defined by the other stars.

In Figure 5, we plot the absolute value of the largest differential velocity we observed for each star in our sample against the period and against the amplitude in the V magnitude. Although the velocity amplitude is more appropriate, the lack of velocity curves for many stars limits its usefulness, and the magnitude amplitude provides a good

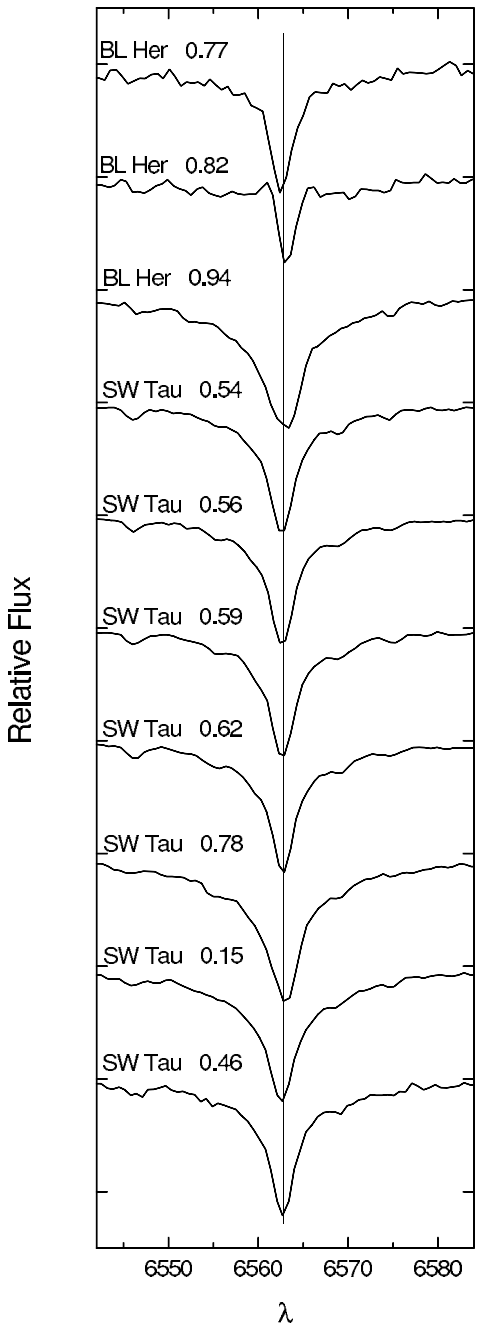

FIG. 3.—Spectra of the stars of class AHB3. The plot has the same format as Fig. 1.

proxy. In selecting the largest velocity, we excluded the spectra with emission for NW Lyr, VZ Aql, and V439 Oph, since the location of the absorption minimum is affected by the distortion of the profile. We have also omitted velocities of emission features. Differential velocities for three type I Cepheids from Vinko et al. (1998), SU Cas, DT Cyg, and SZ Tau, are also plotted. For BL Her, we have used Vinko et al.'s value, since it was larger than ours. Given our limited phase coverage, the velocities must be considered lower limits. Nonetheless, we have sufficient data to provide a clear picture of the behavior of differential velocities in short-period type II Cepheids as compared with classical Cepheids.

It is obvious in Figure 5*a* that our type II Cepheids do not confirm the trend toward small differential velocities at shorter periods that was suggested by Figure 19 of Vinko et al. (1998). Similarly, in Figure 5*b*, we cannot discern the increase in differential velocity with amplitude, which was evident in Figures 20 and 21 of Vinko et al. However, that trend could simply be obscured by our use of lower limits for the differential velocities. Most of our type II Cepheids exhibit differential velocities comparable with or larger than the 10 day stars in the previous sample in spite of being lower limits. There is no apparent separation among the AHB1, AHB2, and AHB3 stars. On the other hand, the classical Cepheids (Cδ and SA) all exhibit smaller differential velocities except for AU Peg and V351 Cep, where $|\Delta\mathrm{Vel}| \geq 30$ km s^{-1}. However, AU Peg is classified as CWB in the GCVS and has generally been regarded as a type II Cepheid, albeit a peculiar one (as discussed by Vinko et al. 1998), while V351 Cep is classed in the GCVS as CWB. Hence, there is reason to question the identification of these stars as classical Cepheids.

We conclude that the short-period type II Cepheids have very dynamic atmospheres compared with classical Cepheids and even compared with longer period stars. In spite of our sparse phase coverage, we see a reasonable separation between the two types of Cepheids. This suggests that measurement of velocity differentials is a promising technique for distinguishing between them at short period.

3.2. *Line Emission*

There are a few instances of obvious emission in our spectra, in particular, in NW Lyr at phase 0.81 (Fig. 2*a*), VZ Aql at phase 0.76 (Fig. 2*b*), and V439 Oph at phases 0.81 and 0.84 (Fig. 2*c*). Weak emission possibly occurs in several other cases, but it is clearly much less certain. Examples are the spectra of BL Her at phase 0.82 (Fig. 3, which is consistent with the spectra presented by Gillet et al. 1994 and Vinko et al. 1998), NW Lyr at phase 0.88 (Fig. 2*a*), and V477 Oph at phase 0.00 (Fig. 2*d*). Thus among 68 spectra of 18 type II Cepheids, mostly taken during phases when emission is most likely, there are only four cases of strong emission features and several possible cases of weak or marginal emission.

We might expect instances when there is no obvious emission but filling of the line will decrease the absorption depth or strength. We will use the central depth of Hα (col. [7] of Table 2) to investigate this. Because other factors have a large influence on the equivalent width, it turned out to be of little value for this purpose. More than 75% of the line depths are between 0.45 and 0.65. In a plot of depth versus phase, all of the instances of depths less than 0.45 fall between phase 0.60 and maximum light. This strengthens the hypothesis that the shallow lines are due to filling by emission. There are 16 spectra that lack obvious emission but that have line depths less than 0.45 in Table 2; we will refer to this as incipient emission. These spectra include two in which we suspected weak emission, BL Her at phase 0.82 and V477 Oph at phase 0.00.

Of the 20 spectra with obvious emission or incipient emission, 16 are from six stars classed as AHB2 (V745 Oph, NW Lyr, V971 Aql, VZ Aql, V439 Oph, and V477 Oph), one from a star classed as AHB1 (CE Her), one from a star classed as AHB3 (BL Her), and two from stars with light curves classed as classical Cepheids (AU Peg and BC Aql).

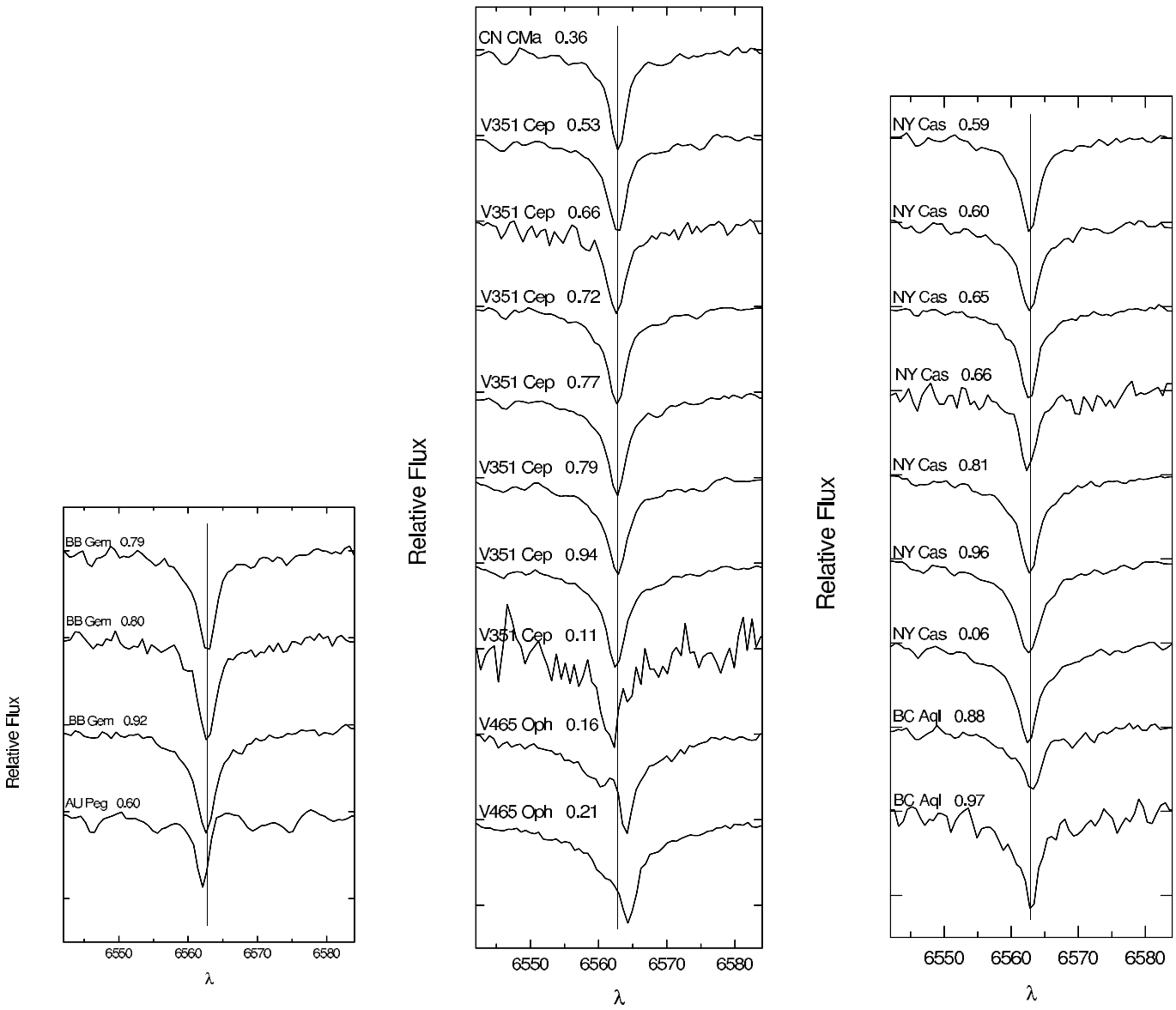

FIG. 4.—Spectra of stars classed as SA or Cδ. The plot has the same format as Fig. 1.

As noted above, there is reason to regard AU Peg as a type II Cepheid. BC Aql is classed as CEP in the GCVS, and the shallowness of Hα may indicate that it is a type II Cepheid in spite of its light-curve morphology.

Of the spectra of AHB2 stars, almost half (16 out of 35 spectra) show emission or incipient emission. The proportion rises to 60% (15 out of 25), if we consider only spectra taken during rising light. Only one spectrum with emission falls outside of rising light (V971 Aql at phase 0.67), and even that one is within the uncertainties of the adopted phase of minimum. On the other hand, only one spectrum out of 10 during rising light for an AHB1 star and one out of four for an AHB3 star show incipient emission. We conclude that emission is common in ABH2 stars during rising light but unusual or perhaps absent in AHB1 stars. We cannot reach a conclusion with regard to the AHB3 stars due to the small number of spectra.

In Figure 6, we have plotted light curves for the seven AHB2 stars using photometry from the sources cited in Table 1. The phases of our spectra are indicated by dashes under the light curves. Each is labeled according to the type of Hα profile observed as follows: "e" indicates obvious emission; "(e)" denotes incipient emission as indicated by line depth; "a" indicates an absorption line of normal depth. We should note that the phasing for V971 Oph is somewhat uncertain due to the paucity of recent photometry.

It can be seen that emission or incipient emission occurred near the strong light-curve bump in all cases. On the other hand, for six of the seven stars in Figure 6, the spectra lacking emission were all taken at other phases. Based on this, we conjecture that emission appears for a short time around the bump in AHB2 stars. Note, however, that the phases of the onset and disappearance of emission relative to the bump shows some variation among the six stars. This may be due, at least in part, to changes from one cycle to another in the pulsation as suggested by the scatter in some of the light curves.

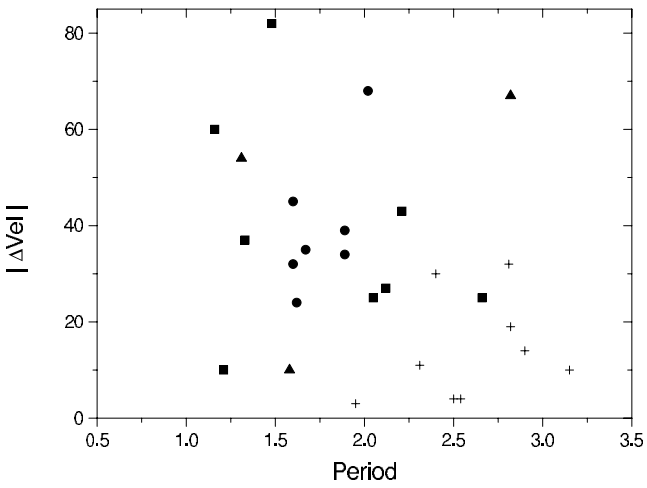

FIG. 5*a*

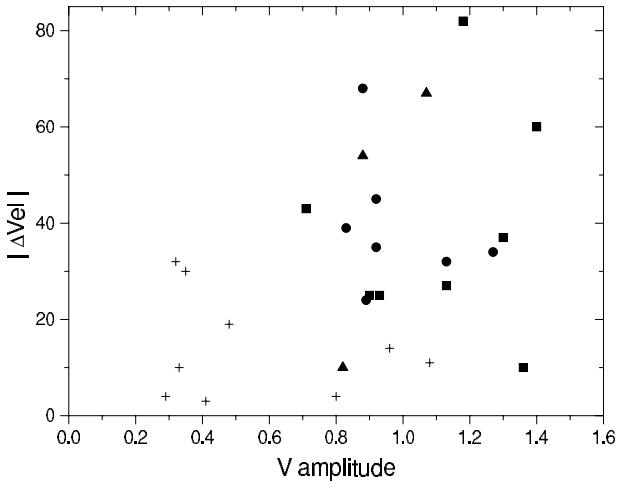

FIG. 5*b*

FIG. 5.—(*a*) Absolute value of the largest observed difference between the velocity of Hα and the metal lines, |ΔVel|, plotted against the period. (*b*) Plot of |ΔVel| against the amplitude of the *V* magnitude. In both plots, the symbols denote the types of the stars as follows: squares, AHB1; circles, AHB2; triangles, AHB3; crosses, Cδ and SA.

Of the seven AHB2 stars, only V714 Cyg gives no indication of Hα emission. We emphasize that the spectra cover the part of the light curve where emission occurred for other AHB2 stars. Noting that the classification of V714 Cyg is uncertain, we suggest that V714 Cyg is not, in fact, an AHB2 star.

3.3. *Line Doubling and Asymmetry*

Doubling of the core of Hα has been reported in at least one short-period type II Cepheid, BL Her (Gillet et al. 1994; Vinko et al. 1998). It is also apparent in our spectrum of MQ Aql (Fig. 1*a*), where the two components are separated by about 100 km s^{-1}. Our Hα profile for BF Ser (also Fig. 1*a*) exhibits a shoulder on one side, which suggests a second component about 90 km s^{-1} longward of the deepest part of the core. Given the resolution of most of our spectra, 2 Å or 90 km s^{-1} at Hα, we cannot detect multiple components of the line core spaced much more closely than this and, in fact, the doubling in BF Ser is only marginally detected. Hence, we have added two more stars to the list of short-period type II Cepheids with known core doubling but cannot use our spectra to comment on the prevalence or location in the cycle of this phenomenon.

Asymmetries are apparent in a number of the profiles displayed in Figures 1–4. Many of these are also profiles that show a significant redshift in the core. In some cases, e.g., NW Lyr at phases 0.88 and 0.93, VZ Aql at phase 0.92, V745 Oph at phase 0.99, and V477 Oph at phase 0.11, these spectra are from stars with emission and are at phases close in the cycle to the emission. This suggests that the asymmetry and the redshift may be due, at least in part, to weak emission on the blueward side of the line core. On the other hand, asymmetries can be seen in stars with no other indication of emission such as UY Eri at phase 0.93. These may be the result of the velocity field in the photosphere.

3.4. *Conclusions*

Christy (1968) showed that when the envelope of a pulsational model begins expansion, a compression wave is driven into the star and reflects from the core. This echo may reappear in the outer envelope during the next cycle and produce a secondary bump in the velocity and light curves. Subsequently, Carson, Stothers, & Vermury (1981) constructed nonlinear models specifically for short-period type II Cepheids and found that, in addition to the bumps generated by the Christy mechanism, there were others related to shocks. In particular, a shock-generated bump appeared in some models during rising light, reminiscent of the AHB2 stars. This may account for the large differential velocities we observed and for the emission lines seen in the AHB2 stars. Thus, the behavior of the Hα profile is of interest in confirming the mechanism responsible for the light-curve bumps in these stars and potentially in providing constraints for the parameters of models of short-period type II Cepheids. It may also provide a basis for determining the basic stellar parameters of AHB2 stars from models and for distinguishing them from AHB1 and AHB3 models.

We are grateful to the staffs of Kitt Peak National Observatory and Apache Point Observatory for their help in obtaining the data used here. We made extensive use of the McMaster Cepheid Photometry and Radial Velocity Data Archive in both the selection of stars for the program and in locating photometric data for use in this paper. We are appreciative of the efforts on the part of Douglas Welch in providing this resource. This work is supported in part by NSF grant AST 00-97353.

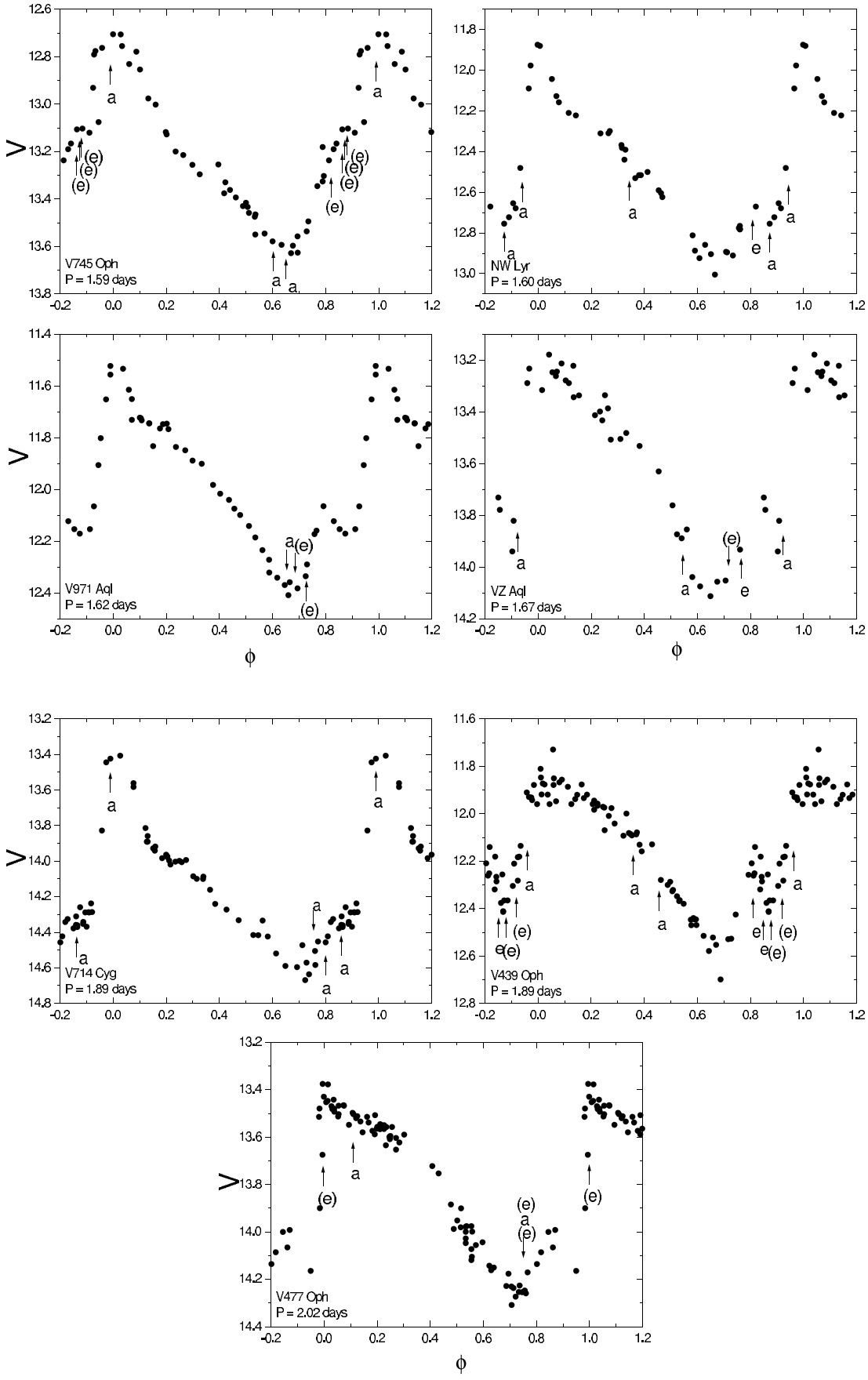

FIG. 6.—*V* light curves for the AHB2 stars. Data are from the sources referenced in Table 1. The phases of our spectra are indicated by short vertical lines under the light curves. The letters indicate the presence of emission as follows: "e," strong emission; "(e)," incipient emission as indicated by line filling; "a," absorption profile with no apparent emission component.

REFERENCES

Abt, H. A., & Hardie, R. H. 1960, ApJ, 131, 155
Barnes, T. F., Fernley, J. A., Frueh, M. L., Navas, J. G., & Moffett, T. J. 1997, PASP, 109, 645
Berdnikov, L. N. 1987, Perem. Zvezdy, 22, 530
———. 1992a, Astron. Astrophys. Trans., 2, 31
———. 1992b, Astron. Astrophys. Trans., 2, 43
———. 1992c, Astron. Astrophys. Trans., 2, 107
———. 1992d, Astron. Astrophys. Trans., 2, 157
———. 1992e, AZh Pis'ma, 18, 325
———. 1993, AZh Pis'ma, 19, 210
Berdnikov, L. N., & Turner, D. G. 1995, AZh Pis'ma, 21, 803
Bednikov, L. N., & Voziakova, O. V. 1995, AZh Pis'ma, 21, 348
Carson, T. R., Stothers, R., & Vermury, S. K. 1981, ApJ, 244, 230
Christy, R. F. 1968, QJRAS, 9, 13
Diethelm, R. 1983, A&A, 124, 108
———. 1986, A&AS, 64, 261
———. 1990, A&A, 239, 186
Diethelm, R., & Tammann, G. 1982, A&AS, 47, 335
Duerinck, R. 1948, Louvin Pub., No. 109
Gillet, D., Burki, G. Chatel, A. Duquennoy, A., & Lèbre, A. 1994, A&A, 286, 508
Harris, H. C. 1980, Ph.D. thesis, Univ. Washington
———. 1981a, AJ, 86, 707
———. 1981b, AJ, 86, 719
Harris, H. C., & Wallerstein, G. 1984, AJ, 89, 379
Henden, A. A. 1980, MNRAS, 192, 621
———. 1996, AJ, 112, 2757
Joy, A. H. 1949, ApJ, 110, 105
Kholopov, P. N. 1985, General Catalogue of Variable Stars, Vols. 1 and 2 (4th ed.; Moscow: Nauka)
———. 1987, General Catalogue of Variable Stars, Vol. 3 (4th ed.; Moscow: Nauka)
Kiss, L. L. 1998, MNRAS, 297, 825
Kraft, R. P., Camp, D. C., & Hughes, W. T. 1959, ApJ, 130, 90
Kwee, K. K., & Diethelm, R. 1984, A&AS, 55, 77
Lèbre, A., & Gillet, D. 1992, A&A, 255, 221
Loomis, C. G., & Schmidt, E. G. 1989, ApJ, 347, L77
Loomis, C. G., Schmidt, E. G., & Simon, N. R. 1988, MNRAS, 235, 1059
Massey, P., DeVeny, J., Jennuzi, B., & Carder, E. 2000, Low-to-Moderate Resolution Optical Spectroscopy Manual for Kitt Peak (Tucson: NOAO)
McMillan, R., Hastings, N. C., & Holtzman, J. 2002, Double Imaging Spectrograph (Sunspot: APO)
Moffett, T. J., & Barnes, T. F. 1984, ApJS, 55, 389
Pollard, K. R., Cottrell, P. L., Lawson, W. A., Lbrow, M. D., & Tobin, W. 1997, MNRAS, 286, 1
Preston, G. W., & Kilston, S. D. 1967, ApJ, 148, 787
Schmidt, E. G. 1970, ApJ, 162, 871
Schmidt, E. G., Chab, J. R., & Reiswig, D. E. 1995, AJ, 109, 1239
Schmidt, E. G., & Reiswig, D. E. 1993, AJ, 106, 2429
Schmidt, E. G., & Seth, A. 1996, AJ, 112, 2769
Sturch, C. R. 1966, PASP, 78, 210
Szabados, L. 1977, Mitt. Sternw. Ung. Akad. Wiss. Budapest, 70
Vinko, J., Evans, N. R., Kiss, L. L., & Szabados, L. 1998, MNRAS, 296, 824